Macromolecules

Article

Cite This: Macromolecules 2019, 52, 3995−4007

pubs.acs.org/Macromolecules

Deswelling of Microgels in Crowded Suspensions Depends on Cross-Link Density and Architecture

Andrea Scotti,*[,†] Alan R. Denton,[‡] Monia Brugnoni,[†] Judith E. Houston,[§,∥] Ralf Schweins,[⊥] Igor I. Potemkin,[#,&,%] and Walter Richtering*[,†,@]

[†]Institute of Physical Chemistry, RWTH Aachen University, 52056 Aachen, Germany

[‡]Department of Physics, North Dakota State University, Fargo, North Dakota 58108-6050 United States

[§]Jülich Centre for Neutron Science (JCNS) at Heinz Maier-Leibnitz Zentrum (MLZ), Forschungszentrum Jülich GmbH, Lichtenbergstr. 1, 85748 Garching, Germany

[∥]European Spallation Source ERIC, Box 176, SE-221 00 Lund, Sweden

[⊥]Institut Laue-Langevin ILL DS/LSS, 71 Avenue des Martyrs, F-38000 Grenoble, France

[#]Physics Department, Lomonosov Moscow State University, 119991 Moscow, Russian Federation

[&]DWI - Leibniz Institute for Interactive Materials, Aachen 52056, Germany

[%]National Research South Ural State University, Chelyabinsk 454080, Russian Federation

[@]JARA, Jülich Aachen Research Alliance, 52056 Aachen, Germany

Supporting Information

ABSTRACT: Microgels are nanometer-to-micrometer-sized cross-linked polymer networks that swell when dispersed in a good solvent. These soft colloids have emerged as versatile building blocks of smart materials, which are distinguished by their unique ability to adapt their behavior to changes in external stimuli. Using X-ray and neutron scattering and molecular simulation methods, we systematically measured and modeled the response to crowding of compressible, deformable microgels with varying cross-link densities and internal architectures. Our experiments and simulations demonstrate that incorporating a solvent-filled cavity during chemical synthesis provides an independent means of controlling microgel swelling that complements the influence of changing cross-link density. In other words, knowledge of the content of cross-links alone cannot be used to define microgel softness, but microgel architecture is another key property that affects softness. These results are potentially important for biomedical applications, such as drug delivery and biosensing.

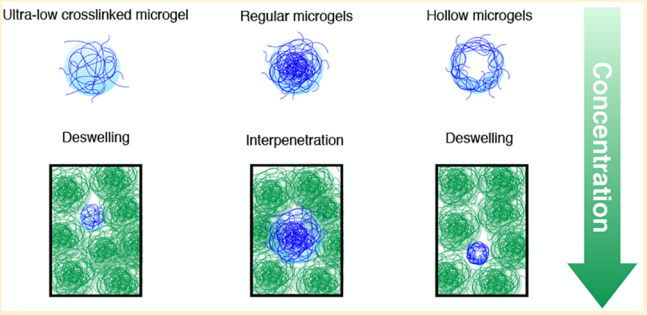

INTRODUCTION

The capacity of soft colloidal particles to respond to crowding by deforming, isotropically shrinking, or interpenetrating strongly affects both the equilibrium and dynamical properties of many soft materials. Understanding which response mechanism dominates in concentrated suspensions is fundamental to predicting the macroscopic behavior of soft matter and designing new materials with desired properties,[1,2] e.g., for biomedical applications.[3,4] Exploiting tunable softness of colloidal building blocks is also vital for the pharmaceutical,[5] oil recovery,[6] and coatings[7] industries, where flow properties must be carefully controlled. For example, materials whose constituent particles mainly interpenetrate show a divergence in the zero-shear viscosity at concentrations higher than materials whose particles preferentially shrink.[8,9] Moreover, gaining fine control over yield stress will facilitate using colloidal suspensions as supports for 3D printing.[10−12]

Microgels and nanogels, microscopic or nanoscopic cross-linked polymer networks swollen in a good solvent,[2,13] have attracted increasing attention as building blocks for soft materials with tunable properties. When solvent is expelled in response to variations in external stimuli, such as temperature[14] or pH,[15] microgels can undergo a phase transition from a swollen soft colloid to a collapsed rigid nanoparticle. The size and structure of the collapsed microgels are strongly influenced by the amount of cross-linker used during the synthesis.[2,16,17] In their swollen state, microgels are soft objects that adapt their size and shape according to concentration and dimensionality. The ability of microgels to deform is crucial when they are confined at an interface.[18,19] Depending on cross-link content, ultrasoft microgels exhibit behavior typical of flexible polymers

Received: April 9, 2019
Revised: May 9, 2019
Published: May 23, 2019

DOI: 10.1021/acs.macromol.9b00729
Macromolecules 2019, 52, 3995−4007

in two dimensions, but not in bulk.[20] Furthermore, ultrasoft microgels are intriguing materials for mimicking biological structures, such as platelets.[21]

More generally, softness is the fundamental characteristic that makes microgels suitable for many different technologies, e.g., sensor applications,[22] paints and coatings,[23] and substrates for cell migration and growth.[24] Moreover, advances in synthesis protocols have made possible *hollow* microgels via a two-step synthesis and the use of sacrificial cores.[25−27] Hollow microgels, which have a solvent-filled cavity in their center, are ideal candidates as nanocarriers for drug delivery.[28,29] Because the degree of swelling of such nanocarriers is fundamental in uptake and release processes, determining whether hollow microgels deswell or interpenetrate at high concentration is key to optimizing their efficiency for drug delivery.[30] All of these applications require fine control over the behavior of microgels in concentrated environments and the ability to predict *a priori* how the soft building blocks react to increasing concentration. Therefore, a deeper understanding of the factors that make microgels soft is pivotal to development of new materials.

In addition to their importance in the development of responsive soft materials and interfaces, microgels have been used to address fundamental questions regarding both liquid-to-solid and solid-to-solid transitions.[31−37] Microgel softness has been shown to play a fundamental role in the formation of strong glasses,[34] in which the suspension viscosity shows a superexponential increase with concentration.[35] Similarly, the softness of microgels strongly affects the liquid-to-crystal transition. Suspensions of microgels crystallize at higher volume fraction with respect to hard spheres[38−40] due to their external fuzzy shell.[41] Varying the amount of cross-linker agent used during the precipitation polymerization controls the distribution of cross-links within the polymer network and thus, the softness of the microgels.[42] It has been observed that microgels with an extended fuzzy shell can form a metastable body-centered-cubic lattice,[43,44] in contrast to hard spheres and stiffer microgels that crystallize in face-centered-cubic (fcc) crystals.

These examples highlight how softness makes microgels substantially different from hard, incompressible spheres. This difference is related to the capability of the microgels to be compressed, deformed, or interpenetrated by their neighbors, depending on their concentration in the suspension.[14,45−51] By understanding which of these response mechanisms is dominant, and at what concentrations, a better understanding of the macroscopic behavior of microgel suspensions and, more generally, the role of softness in the liquid-to-solid phase transition can be achieved.

Recently, many efforts have been devoted to studying microgels in concentrated or overcrowded suspensions, which have shown contrasting results. Large microgels embedded in a majority of smaller microgels deswell to the size of the latter, depending on the concentration of the suspension.[47] This mechanism has a significant impact on the phase behavior of binary and polydisperse suspensions of microgels, allowing crystals to form at size polydispersities for which hard spheres can form only glasses.[49] In contrast, once microgels of the same size and softness are mixed together, interpenetration has been observed to be more prevalent,[48] while compression is only a marginal response.[14,46]

The aforementioned studies were all based on small-angle neutron scattering (SANS). Because of both the size polydispersity and the instrument resolution, deformations of microgels, resulting in aspherical shapes, can produce effects that are not measurable within the SANS sensitivity. Direct imaging of larger microgels highlighted that deformation is also present once the microgels are squeezed by their neighbors. Nevertheless, a variety of outcomes are reported: in a mixture of a few large and a majority of smaller microgels, the former are compressed without deformations;[45] in suspensions of microgels with the same size and softness, faceting is evident. Whether faceting occurs before[50] or after[51] isotropic compression, however, is not yet clear.

In this contribution, we study the response of microgels to overcrowded environments and vary the degrees of softness by employing microgels of different cross-linking densities as well as introducing microgels with different architectures. We investigate how the softness of the network and the presence of a solvent-filled cavity affect deswelling of the microgels when squeezed together.

EXPERIMENTAL SECTION

Synthesis. The synthesis of ultra-low cross-linked poly(*N*-isopropylacrylamide), pNIPAM ($[C_6H_{11}NO]_n$), microgels was previously described.[52] The use of sodium dodecyl sulfate (SDS) during polymerization enabled the achievement of small particle sizes. Briefly, 3.9606 g of NIPAM and 0.1802 g of SDS were dissolved in 495 mL of filtered (0.2 μm regenerated cellulose, RC, membrane filter) double-distilled water. The monomer solution was purged with nitrogen under stirring at 100 rpm while heated to 70 °C. Separately, 0.2108 g of potassium peroxydisulfate (KPS) in 5 mL of filtered double-distilled water was degassed for 1 h. The polymerization was initiated by transferring the KPS solution with a nitrogen-washed syringe equipped with a needle into the monomer solution. The reaction was allowed to proceed for 4 h under constant nitrogen flow at 70 °C and 100 rpm. The resulting microgels were purified by 3-fold ultracentrifugation at 50000 rpm and subsequent redispersion in fresh water. Lyophilization was applied for storage.

The synthesis of hollow microgels relies on the generation of silica core−pNIPAM shell microgels with subsequent core dissolution. The sacrificial silica cores were obtained by the well-known Stöber synthesis.[53] After heating 700 mL of ethanol under reflux to 60 °C, we added 63 mL of 28−32% ammonia solution. Following 10 min of equilibration, the reaction was started by adding 30 mL of tetraethyl orthosilicate (TEOS). After 24 h reaction time, the nanoparticles were surface-modified with 3-methacryloxypropyltrimethoxysilane (MPS).[25] The silica cores were purified by 3-fold centrifugation at 5000 rpm and redispersion in fresh ethanol. The solvent was evaporated for storage.

For the syntheses of silica core−pNIPAM shell microgels, 1.61 g of the silica nanoparticles was redispersed in 5 mL of ethanol. The suspension was ultrasonicated to prevent silica aggregates during the shell polymerization and then transferred to the monomer solution. For the 5 mol % cross-linked shell, 1.1315 g of NIPAM, 81.1 mg of *N*,*N*′-methylenebis(acrylamide) (BIS), and 144.2 mg of SDS (for the 2.5 mol % cross-linked shell, 1.2412 g of NIPAM, 43.4 mg of BIS, and 144.2 mg of SDS) were dissolved in 245 mL of filtered double-distilled water. The solutions were purged with nitrogen under stirring at 200 rpm and heated to 60 °C. Simultaneously, a solution of 105.4 mg of KPS in 5 mL of filtered double-distilled water was degassed. To start the polymerization, the initiator solution was rapidly transferred into the monomer solution. The reaction was allowed to proceed for 4 h under constant nitrogen flow and stirring at 60 °C. The core−shell microgels were purified by 3-fold ultracentrifugation at 30000 rpm and redispersion in fresh water. Lyophilization was performed for storage.

To generate hollow microgels, the silica cores were dissolved by means of a sodium hydroxide (NaOH) solution.[54] Briefly, 1.100 g of the core−shell microgels was redispersed in 50 mL of water. After

DOI: 10.1021/acs.macromol.9b00729
Macromolecules 2019, 52, 3995−4007

complete dispersion, 50 mL of a 0.1 M NaOH solution was added and allowed to react for 4 days. Dialysis was applied to remove the remaining silica and neutralize the suspension. Finally, the resulting hollow microgels were centrifuged at 50000 rpm to reduce the total volume, and lyophilization was performed for storage.

To synthesize the 5 mol % cross-linked pNIPAM microgels, we dissolved 8.4870 g of NIPAM, 0.6090 g of BIS, and 0.0560 g of SDS in 495 mL of filtered double-distilled water. To produce the 2.5 mol % cross-linked pNIPAM microgels, we dissolved 9.0516 g of NIPAM, 0.3162 g of BIS, and 0.0900 g of SDS in 395 mL of filtered double-distilled water. The solutions were heated to 60 °C and degassed by purging with nitrogen for 1 h under constant stirring at 300 rpm. Meanwhile, an initiator solution of 0.2108 g of KPS (5 mol % microgels) or 0.1687 g of KPS (2.5 mol % microgels) in 5 mL of filtered double-distilled water was degassed separately. To initiate the reactions, the initiator solution was transferred rapidly into the monomer solution. The polymerizations were allowed to proceed for 4 h. Ultracentrifugation at 30000 rpm was used for purification and lyophilization for storage.

The deuterated regular 5 mol % cross-linked microgels were synthesized by precipitation polymerization. We dissolved 1.5072 g of deuterated NIPAM (D7-pNIPAM, $[C_6D_7H_4NO]_n$), 0.1021 g of BIS, and 20.2 mg of SDS in 83 mL of filtered double-distilled water. The solution was purged with nitrogen for 1 h while heated to 60 °C under constant stirring. The polymerization was started by rapid addition of the degassed initiator solution (37.1 mg of KPS in 5 mL of water). The reaction was allowed to proceed for 4 h under constant stirring. Subsequently, the microgels were purified by 3-fold centrifugation at 50000 rpm and redispersion in fresh water. For storage, lyophilization was applied.

Small-Angle X-ray Scattering (SAXS). The SAXS measurements were performed on the cSAXS instrument at the Swiss Light Source, Paul Scherrer Institut (Villigen, Switzerland) using an X-ray wavelength $\lambda = 0.143$ nm with an error of 0.02% over λ resolution. To cover the q range of interest, a sample to detector distance of 7.12 m was set. The area illuminated by the collimated beam was about 200 μm × 200 μm. The instrument mount had a 2D detector with a pixel size of 172 μm and 1475 × 1679 pixels.

Small-Angle Neutron Scattering (SANS). The SANS measurements, using the KWS-2 instrument operated by JCNS at the Heinz Maier-Leibnitz Zentrum (MLZ, Garching, Germany), were performed at three configurations to cover the q range of interest: sample detector distance $d_{SD} = 20$ m with neutron wavelength $\lambda = 1$ nm; $d_{SD} = 8$ m with $\lambda = 0.5$ nm; and $d_{SD} = 2$ m with $\lambda = 0.5$ nm. Because of the velocity selector, the resolution in λ was 10%. The instrument was equipped with a ^{3}He detector with a pixel size of <8 mm.

The q range of interest for the measurements performed with the D11 instrument at the Institut Laue-Langevin (ILL, Grenoble, France) was covered using three configurations: $d_{SD} = 34$ m with $\lambda = 0.6$ nm; $d_{SD} = 8$ m with $\lambda = 0.6$ nm; and $d_{SD} = 2$ m with $\lambda = 0.6$ nm. Because of the velocity selector, the resolution in λ was 9%. The instrument was equipped with a ^{3}He detector with a pixel size of 7.5 mm.

FLORY–HERTZ MODEL OF MICROGELS

We consider a binary mixture of hollow and regular microgels dispersed in a solvent. Each hollow microgel, consisting of $N_{mon,h}$ monomers and $N_{ch,h}$ cross-linked chains, has in its collapsed state a cavity (inner) radius c_{0h} and outer radius R_{0h} and in its swollen state a cavity radius c_h and outer radius R_h. Each regular microgel, consisting of $N_{mon,r}$ monomers and $N_{ch,r}$ chains, has collapsed radius R_{0r} and swollen radius R_r. For simplicity, we assume that the cross-links are uniformly distributed throughout the particle volume. Under the assumption that for a particle in the collapsed state monomers are random-close-packed, the monomer numbers are related to the collapsed radii according to

$$N_{mon,h} = 0.63\frac{R_{0h}^3 - c_{0h}^3}{r_{mon}^3}$$
$$N_{mon,r} = 0.63\left(\frac{R_{0r}}{r_{mon}}\right)^3 \quad (1)$$

where $r_{mon} \simeq 0.3$ nm is a typical monomer radius. The regular microgels have a linear swelling ratio $\alpha_r = R_r/R_{0r}$, defined as the ratio of the swollen radius to a reference radius, which we choose to be the collapsed radius. For the hollow microgels, to allow for independent variations of the inner and outer radii, we define the linear swelling ratio via the volume ratio of the swollen and collapsed particles:

$$\alpha_h = \left(\frac{v_h}{v_{0h}}\right)^{1/3} = \left(\frac{\alpha_{out,h}^3 - \gamma^3\alpha_{in,h}^3}{1 - \gamma^3}\right)^{1/3} \quad (2)$$

where $\alpha_{in,h} \equiv c_h/c_{0h}$ and $\alpha_{out,h} \equiv R_h/R_{0h}$ are the inner and outer swelling ratios, respectively, and $\gamma \equiv c_{0h}/R_{0h}$ is the ratio of the collapsed inner and outer radii.

In a coarse-grained model, we describe swelling of microgels via the Flory–Rehner theory of polymer networks.[55−57] Combining mixing entropy, polymer–solvent interactions, and elastic free energy, the free energy of a microgel of swelling ratio α (= α_h or α_r) is

$$\beta F(\alpha) = N_{mon}[(\alpha^3 - 1)\ln(1 - \alpha^{-3}) + \chi(1 - \alpha^{-3})] + \frac{3}{2}N_{ch}(\alpha^2 - \ln\alpha - 1) \quad (3)$$

where $\beta \equiv 1/(k_BT)$ at temperature T, N_{mon} and N_{ch} are the monomer and chain numbers of the particle, and χ is the Flory solvency parameter, associated with polymer–solvent interactions. When applying the Flory–Rehner theory, choosing the reference particle radius to be the collapsed radius is equivalent to choosing the reference polymer volume fraction to be the random-close-packed volume fraction of monomers in the collapsed state (eq 1). Our choice is consistent with the experimental synthesis, in which cross-linking occurs at temperatures sufficiently high that the particles are in their collapsed states. Previous studies[58,59] that have successfully fit the Flory–Rehner theory to light scattering data for swelling of thermoresponsive microgels have determined that the volume phase transition can be accurately predicted only if the Flory solvency parameter is treated as a function of temperature and the polymer volume fraction ϕ, following the form

$$\chi(T, \phi) = \frac{1}{2} - A\left(1 - \frac{\theta}{T}\right) + C\phi + D\phi^2 \quad (4)$$

where θ is the theta temperature and A, C, and D are fit parameters. pNIPAM microgels in water are typically characterized by $\chi < 0.5$, despite θ being near room temperature.[58,59]

Interactions between a pair of particles of respective (outer) radii R_i and R_j are modeled via a Hertzian effective pair potential[60]

$$v_H(r_{ij}) = \begin{cases} \epsilon_{ij}\left(1 - \frac{r_{ij}}{R_i + R_j}\right)^{5/2}, & r_{ij} < R_i + R_j \\ 0, & r_{ij} \geq R_i + R_j \end{cases} \quad (5)$$

DOI: 10.1021/acs.macromol.9b00729
Macromolecules 2019, 52, 3995−4007

where r_{ij} is the center-to-center separation of particles i and j. It should be noted that the Hertz potential, although originally intended to model the energy of deformation of elastic spheres, can also be interpreted as a free energy cost associated with interpenetration. In this sense, our model does not distinguish between shape deformation (faceting) and interpenetration of interacting microgels.

Neglecting any influence of the cavity on the strength of interactions involving hollow particles, the amplitudes of the pair potentials are given by[60]

$$\epsilon_{ij} = \frac{8}{15}\left(\frac{1-\nu_i^2}{Y_i} + \frac{1-\nu_j^2}{Y_j}\right)^{-1}(R_i + R_j)^2(R_iR_j)^{1/2} \tag{6}$$

depending on the gel elastic properties through Young's moduli Y_i and the Poisson ratios ν_i. Assuming equal Poisson ratios ν for hollow and regular microgels, we have

$$\epsilon_{ij} = \frac{8}{15}\frac{Y_iY_j}{Y_i + Y_j}\frac{(R_i + R_j)^2}{1-\nu^2}(R_iR_j)^{1/2} \tag{7}$$

Using the scaling prediction for polymer gels in good solvents,[61] namely, that the bulk modulus scales linearly with both temperature and cross-linker density, i.e., $Y_r \sim k_BTN_{ch,r}/R_r^3$ and $Y_h \sim k_BTN_{ch,h}/(R_h^3 - c_h^3)$, we can write

$$\beta\epsilon_{ij,rr} = C\frac{N_{ch,r}(R_{ir} + R_{jr})^2(R_{ir}R_{jr})^{1/2}}{(1-\nu^2)(R_{ir}^3 + R_{jr}^3)} \tag{8}$$

$$\beta\epsilon_{ij,rh} = C\frac{N_{ch,r}N_{ch,h}(R_{ir} + R_{jh})^2(R_{ir}R_{jh})^{1/2}}{(1-\nu^2)[N_{ch,r}(R_{jh}^3 - c_{jh}^3) + N_{ch,h}R_{ir}^3]} \tag{9}$$

$$\beta\epsilon_{ij,hh} = C\frac{N_{ch,h}(R_{ih} + R_{jh})^2(R_{ih}R_{jh})^{1/2}}{(1-\nu^2)(R_{ih}^3 - c_{ih}^3 + R_{jh}^3 - c_{jh}^3)} \tag{10}$$

where the proportionality constant C is used to calibrate the model with experiment. The larger the Hertz potential amplitudes (i.e., the stiffer the particles), the more favorable it is for the microgels to deswell to avoid interactions with their neighbors. The total internal energy associated with pair interactions is then given by

$$U = \sum_{i<j=1}^{N_h} v_H(r_{ij}) + \sum_{i<j=1}^{N_r} v_H(r_{ij}) + \sum_{i=1}^{N_h}\sum_{j=1}^{N_r} v_H(r_{ij}) \tag{11}$$

where the sums run over pairs of microgels, and in each term the appropriate amplitude must be taken from eqs 8−10. In our Monte Carlo simulations, changes in U and F determine the acceptance probabilities of microgel trial moves. Although the experimental synthesis yields microgels with a nominal cross-link fraction of 0.05, the actual fraction is likely much smaller. For purposes of illustration, we chose $x_r = 0.001$, implying relatively loosely cross-linked particles. For the calibration factor in eqs 8−10, we chose $C = 10$, corresponding to Young's moduli in the range of 50−100 kPa. Although experimental moduli may be somewhat lower, this choice accentuates the influence of the Hertzian interparticle interactions on deswelling.

RESULTS AND DISCUSSION

Generalized Volume Fraction. To systematically study how the cross-link content and the architecture of a microgel affect its swelling behavior in overcrowded environments, we synthesized different pNIPAM-based microgels via precipitation polymerization: (i) Regular cross-linked pNIPAM microgels, synthesized with different concentrations of cross-linker (5 and 2.5 mol %). These microgels have a dense, more cross-linked core surrounded by a fuzzy soft shell.[17,41,48,49] (ii) Ultra-low cross-linked (ULC) microgels, synthesized without any additional cross-linker agent, in which cross-linking is promoted via atom transfer reactions.[20,52,62,63] ULC microgels are the pNIPAM-based microgels with the lowest amount of cross-links that can be synthesized by precipitation polymerization. (iii) Hollow microgels, i.e., fuzzy spheres with a solvent-filled cavity in their center,[27−29,54,64] synthesized by precipitation polymerization of pNIPAM shells onto sacrificial silica cores. Two different types of hollow microgel were produced by adding 5 and 2.5 mol % cross-linker agents during the synthesis. In both cases the sacrificial silica cores had a radius of 57 ± 1 nm.[65] These five different pNIPAM-based microgels were embedded within a matrix of deuterated, regular 5 mol % cross-linked pNIPAM microgels. The concentration of the H-containing microgels is kept constant in the different suspensions measured, while the number of deuterated microgels varies to change the total concentration.

The concentration of the suspensions is expressed by the generalized volume fraction, ζ, defined as the volume occupied by the microgels in their swollen state divided by the total available volume of the sample. Thus, ζ is directly proportional to the mass concentration, $c = m_{poly}/m_{tot}$, where m_{poly} and m_{tot} are the mass of polymer in suspension and the total mass of the suspension: $\zeta = kc$.[66] The conversion constants, k, for all the microgels were obtained from viscosimetry measurements.[65] The volume fraction of the suspensions is then computed as the sum of the volume fractions of the deuterated microgels plus the ζ of the pNIPAM-based microgels. The latter is kept constant and equal to 0.08 ± 0.01 to avoid interaction between the probed microgels.

Small-Angle X-ray Scattering (SAXS). The arrangement of the deuterated microgels composing the matrix and their nearest-neighbor distance, d_{nn}, as a function of ζ is probed by using SAXS. The scattered intensity of concentrated suspensions, $I(q)$ with q the scattering vector magnitude, is proportional to the product of the form factor, $P(q)$, and the structure factor, $S(q)$:

$$I(q) \propto P(q)S(q) \tag{12}$$

In eq 12, $P(q)$ contains information about the radial distribution and the architecture of the scattering object, while $S(q)$ gives information about the reciprocal arrangement of the microgels in the suspensions. We estimate d_{nn} using the q value of the maximum of the first peak of $I(q)$ or, equivalently, of $S(q)$. The latter is obtained by dividing the measured $I(q)$ by $P(q)$, measured in a dilute suspension, $\zeta \lesssim 0.08$. Despite neglecting the dependence of $P(q)$ on ζ, this approximation does not lead to significant differences (<2%) in the value of $d_{nn} = 2\pi/q_{max}$, with q_{max} being the q value of corresponding to the first peak in $S(q)$.[49]

Figure 1 shows data for d_{nn} as a function of ζ for the suspensions composed of deuterated microgels alone (green left triangles). The red dashed line is a fit of the data with the law describing the expected behavior of d_{nn} in concentrated suspensions: $z\zeta^{-1/3}$, with z as fitting parameter corresponding to the nearest-neighbor distance at $\zeta = 1$.[47−49] Also plotted in Figure 1 are the data corresponding to the nearest-neighbor

DOI: 10.1021/acs.macromol.9b00729
Macromolecules 2019, 52, 3995−4007

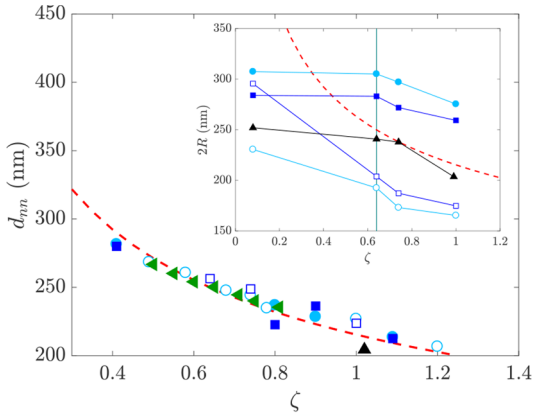

Figure 1. Nearest-neighbor distance, d_{nn}, determined from SAXS as a function of generalized volume fraction, ζ, for deuterated regular 5 mol % cross-linked microgels (green solid left triangles); matrix of deuterated regular 5 mol % with embedded regular 5 mol % cross-linked microgels (cyan solid circles); regular 2.5 mol % cross-linked microgels (blue solid squares); ultra-low cross-linked microgels (black solid triangles); hollow 5 mol % (cyan empty circles); and hollow 2.5 mol % (blue empty squares) cross-linked microgels. The dashed red line is a fit of the data with $d_{nn} = z\zeta^{-1/3}$. All samples were measured at 20.0 ± 0.1 °C. Inset: microgel diameters, $2R$, obtained from SANS, versus ζ. Symbols and red dashed line have the same meanings as in the main figure. The vertical line indicates the volume fraction at random close packing, $\zeta_{rcp} = 0.64$.

distance of the samples composed by the majority of deuterated microgels and a minority of pNIPAM-based microgels. It is clear that the trends of all the data sets are virtually the same and lie on the dashed curve. This proves that, on one hand, a minority of pNIPAM-based microgels do not affect the structure of the matrix of deuterated microgels and, on the other, that in all the samples the microgels are embedded in the same environment. Consequently, the osmotic pressures of all suspensions at the same matrix concentration are virtually the same.

Small-Angle Neutron Scattering (SANS). Because hydrogen and deuterium possess different and opposite scattering length densities, a proper mixture of water and heavy water allows matching the scattering length density of the deuterated microgels.[46−48] The matrix of the regular deuterated 5 mol % cross-linked microgels was contrast-matched using as solvent 90 wt % heavy water in a water/heavy water mixture.[65] Therefore, in eq 12, $S(q) \approx 1 \rightarrow I(q) \propto P(q)$, and the form factors of the embedded microgels were directly measured. The form factor is related to the radial distribution of polymer within a microgels, i.e., the radial density profile, via a Fourier transformation:[24,67]

$$P(q) \propto \Delta\rho \int_V \Phi(r) e^{-iq\cdot r}\, dr \tag{13}$$

where $\Delta\rho$ and $\Phi(r)$ are the scattering contrast between the embedded microgels and the solvent and the radial density profile of the embedded microgels, respectively. Equation 13 relates the density profiles for a fuzzy sphere[41,67] and for a hollow-fuzzy sphere[54,64] to the analytical equations used in this work to fit the form factors of the embedded microgels. In the Supporting Information, we show that the analytical equations of both the fuzzy sphere and the hollow-fuzzy sphere models derive from the Fourier transform of a core−shell particle. The model for a fuzzy sphere[41] is obtained by requiring the internal fuzziness to be zero and the scattering contrast between the solvent and the core to be the same as the scattering contrast between the solvent and the shell.[67] Similarly, the model for the hollow-fuzzy sphere is obtained by imposing that the scattering contrast between the solvent and the core is zero.[27] From the fits, the characteristic lengths, namely the total radius, R, the thickness of the fuzzy shell, σ_{out}, and the inner radius (either radius of the core or radius of the cavity), R_{in}, are obtained and used to draw the radial density profiles. For all investigated microgels, the mass is conserved independently of the swelling state. Therefore, the area under the radial density profile of the collapsed microgels, $\int_0^\infty \Phi(r, T = 40\ °C, \zeta < 0.08)\, r^2\, dr$, has been used to normalize all the curves of the same microgels to obtain the plot of the relative polymer volume fraction within the microgel versus the distance from the microgel center.

We first investigate whether decreasing the concentration of cross-linker agents used during the precipitation polymerization, resulting in fewer cross-links within the microgel network, affects the deswelling/interpenetration of microgels in overcrowded environments. For this aim, the behavior of the 5 and 2.5 mol % cross-linked regular microgels and the ULC microgels is measured once they are embedded in the matrix of the deuterated 5 mol % cross-linked microgels.

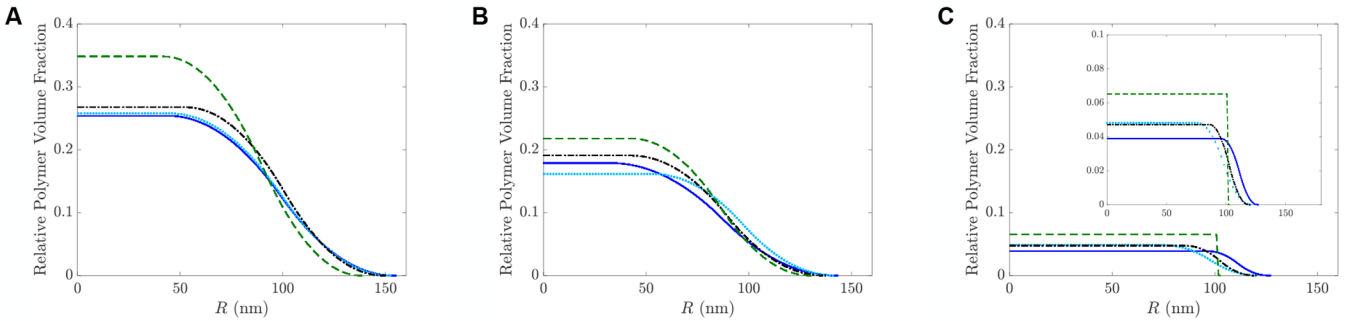

Figure 2. Relative polymer volume fraction within the microgel versus distance from the microgel center for 5 mol % cross-linked regular microgels (A), 2.5 mol % cross-linked regular microgels (B), and ultra-low cross-linked microgels (C). In (A) and (B) the lines correspond to $\zeta = 0.08 \pm 0.01$ (blue solid line), $\zeta = 0.64 \pm 0.02$ (cyan dotted line), $\zeta = 0.74 \pm 0.03$ (black dash-dotted line), and $\zeta = 1.00 \pm 0.04$ (green dashed line). In (C) the lines correspond to $\zeta = 0.08 \pm 0.01$ (blue solid line), $\zeta = 0.64 \pm 0.02$ (cyan dotted line), $\zeta = 0.74 \pm 0.02$ (black dash-dotted line), and $\zeta = 0.99 \pm 0.03$ (green dashed line). The inset is a magnification of the relative polymer volume between 0 and 0.1. All these measurements were conducted at $T = 20.0 \pm 0.1$ °C.

DOI: 10.1021/acs.macromol.9b00729
Macromolecules 2019, 52, 3995−4007

Figure 2A shows the radial density profiles of 5 mol % cross-linked regular microgels. In the swollen state, at 20.0 ± 0.1 °C, the data are reproduced by the fuzzy sphere model (solid blue line).[41,65] When the temperature is well above the volume phase transition temperature (VPTT), 40.0 ± 0.1 °C, the microgels collapse and the box-like profile is obtained from the fit (solid red line in Figure S6). The regular microgel radius R decreases from 154 ± 3 to 84 ± 1 nm.

The cyan dotted line in Figure 2A shows the radial density profile of the microgels at ζ = 0.64 ± 0.02. At this concentration, the microgels make contact with their neighbors. The microgel radius is 152 ± 2 nm, almost identical to that in the dilute state (solid blue line). At ζ = 0.74 ± 0.03, the radius is 148 ± 3 nm, and the radial density profile (black dash-dotted line) is virtually the same as the one at ζ = 0.64 ± 0.02. A further increase of concentration, up to ζ = 1.00 ± 0.04 (green dashed line), causes a more pronounced reduction of the microgel radius to 137 ± 3 nm. The inset in Figure 1 compares the diameters of the probed microgels (cyan solid circles) with the nearest-neighbor distance of the embedding matrix (red dashed line). It is evident that the particle diameters exceed d_{nn} ($2R$ lies above the dashed red line) for the corresponding values of ζ. This behavior indicates that interpenetration is the dominant response to overcrowding, as observed in ref 48.

The response of microgels with lower number of cross-links in their polymer network is studied by probing regular 2.5 mol % cross-linked microgels suspended in a majority of deuterated stiffer regular 5 mol % cross-linked microgels. The radial density profiles of the swollen microgels at 20.0 ± 0.1 °C in a dilute suspension is consistent with a fuzzy sphere with a radius of 142 ± 4 nm (blue solid line in Figure 2B). Once the temperature is increased to 40.0 ± 0.1 °C, the microgel collapses to a size of 68 ± 1 nm and a box-like profile reproduces the data (red solid line in Figure S6).

Once in contact with the 5 mol % cross-linked microgels composing the matrix, at ζ = 0.64 ± 0.02, the radial density profile of 2.5 mol % cross-linked microgels is virtually the same as in the dilute state, with a size of 142 ± 4 nm (cyan dotted line). When the volume fraction rises to 0.74 ± 0.03, the microgels are compressed to a radius of 136 ± 4 nm and external fuzziness is still present. At the highest investigated concentration, ζ = 1.00 ± 0.04, the total radius is 129 ± 2 nm. Similar to the 5 mol % cross-linked microgels, the 2.5 mol % cross-linked microgels are not significantly further compressed; however, at $\zeta \approx 1$ the relative compression of the 2.5 mol % cross-linked microgels is slightly larger than for the 5 mol % cross-linked microgels (Figure S8). This indicates that for networks with a lower number of cross-links as compared to the microgels that provide the overcrowded environments the isotropic compression is more pronounced. Nevertheless, upon comparison of the diameters of the 2.5 mol % microgels (blue solid squares) with the d_{nn} of the matrix of deuterated microgels (red dashed line) in the inset of Figure 1, the former are larger for all the corresponding values of ζ. Therefore, interpenetration is still the dominant response to overcrowding.

The blue and red solid lines in Figure 2C and Figure S6 show the radial density profiles of ULC microgels below and above the VPTT, respectively. At 40.0 ± 0.1 °C, well above the VPTT, a dramatic collapse of the microgel is observed: the radius decreases from 126 ± 1 to 41 ± 1 nm. This strong deswelling is consistent with the fact that the ULC microgels have the lowest number of cross-links for a pNIPAM-based microgel obtained via precipitation polymerization, as also highlighted by the swelling ratio in Figure S10.[65]

The form factor of the ULC microgels, at the highest compression measured, ζ = 0.99 ± 0.03 (black triangles), is shown in Figure 3 and compared to the form factor in the dilute states at ζ = 0.08 ± 0.01 (black circles). In the range between 0.03 and 0.02 nm^{-1}, the former has a less pronounced decay than the latter, indicating that the radial density profile is changed in overcrowded environments.[46−48] The dashed yellow lines represent the fits of the data with the fuzzy sphere model used to plot the radial distributions of the relative polymer volume fraction within the microgel, shown in Figure 2C.

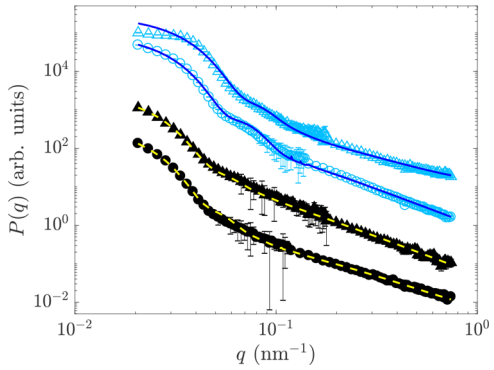

Figure 3. SANS form factor, $P(q)$, versus scattering vector magnitude q for ultra-low cross-linked microgels at ζ = 0.08 ± 0.01 (black circles) and ζ = 0.99 ± 0.03 (black triangles); hollow 5 mol % cross-linked microgels at ζ = 0.08 ± 0.01 (empty circles) and ζ = 1.00 ± 0.04 (empty triangles). All measurements were conducted at T = 20.0 ± 0.1 °C. For clarity, black triangles, empty circles, and empty triangles are shifted up by 10, 10^2, and 10^3, respectively.

For ζ = 0.99 ± 0.03, the dashed green line highlights that the main difference with respect to the swollen state is the compression of the fuzzy shell. Furthermore, the ULC microgels are compressed to a radius of 102 ± 3 nm. For the intermediate concentrations, ζ = 0.64 ± 0.02 and ζ = 0.74 ± 0.02, the radial density profiles (cyan dotted and black dash-dotted lines, respectively) are compressed to 120 ± 2 and 119 ± 3 nm, respectively. The comparison of the diameters of the studied ULC microgels (black solid triangles) to the d_{nn} of the matrix in which they are embedded (red dashed line) shows that d_{nn} is larger than the diameter of the compressed ULC microgels (inset of Figure 1). Therefore, interpenetration is absent, confirming that once microgels with a significant difference in network softness (i.e., in the amount of cross-links) are mixed, compression of the softest microgel is the dominant response.[45,47,49]

From the response to overcrowding of microgels containing different cross-link concentrations, i.e., with polymer networks differing in softness, we can draw two conclusions: (i) interpenetration is the dominant response when microgels synthesized with comparable amount of cross-linker agents and size are mixed together; (ii) microgels with significantly lower cross-link amount as compared to the microgels composing the embedding matrix are preferentially compressed.

To further investigate how the interplay between the microgel architecture and the amount of cross-links of the polymer network affects the behavior of microgels once they

DOI: 10.1021/acs.macromol.9b00729
Macromolecules 2019, 52, 3995−4007

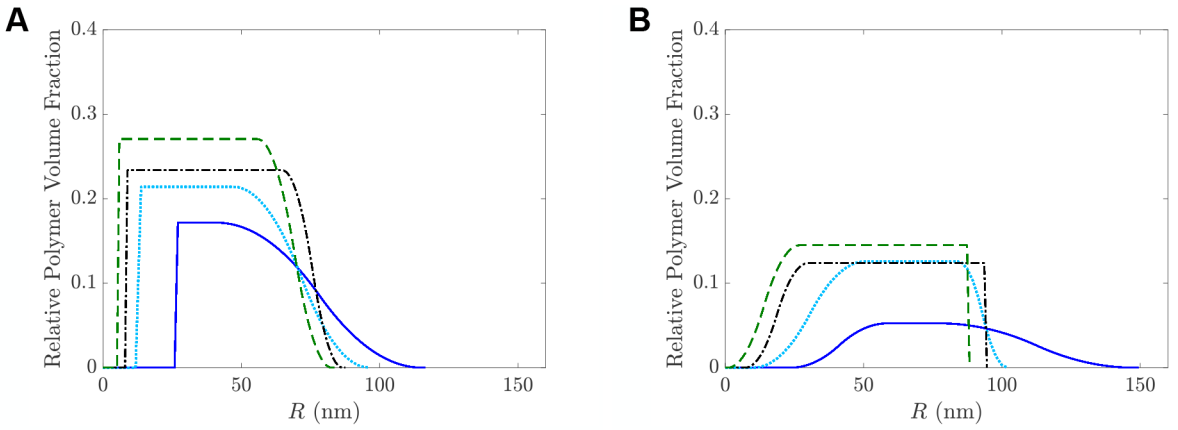

Figure 4. Relative polymer volume fraction within the microgel versus distance from the microgel center for hollow 5 mol % (A) and 2.5 mol % (B) cross-linked microgels. In (A) the lines correspond to $\zeta = 0.08 \pm 0.01$ (blue solid line), $\zeta = 0.64 \pm 0.02$ (cyan dotted line), $\zeta = 0.74 \pm 0.02$ (black dash-dotted line), and $\zeta = 1.00 \pm 0.03$ (green dashed line). In (B) the lines correspond to $\zeta = 0.08 \pm 0.01$ (blue solid line), $\zeta = 0.64 \pm 0.02$ (cyan dotted line), $\zeta = 0.74 \pm 0.03$ (black dash-dotted line), and $\zeta = 1.00 \pm 0.04$ (green dashed line). All these measurements were conducted at $T = 20.0 \pm 0.1$ °C.

are squeezed by their neighbors, hollow microgels with 5 mol % cross-linked shell were embedded within a matrix of the same regular 5 mol % deuterated microgels as used before. Indeed, the presence of a solvent-filled cavity resulting in an inhomogeneous object might significantly affect microgel deswelling.[64]

The form factors of the hollow 5 mol % cross-linked microgels, shown in Figure 3, show significant differences depending on ζ: (i) at $\zeta = 1.00 \pm 0.03$ (empty triangles) the form factor decays for higher q values compared to the dilute state (empty circles); (ii) the kink of $P(q)$ between $0.05 < q < 0.09$ is more pronounced for the dilute suspension (empty circles) than for the microgel embedded within the matrix at $\zeta = 1.00 \pm 0.03$ (empty triangles). These two traits are the consequence of both deswelling and a change in the radial density profile of the scattering object, i.e., collapse of the fuzzy shell and the decrease of the cavity radius, with increasing ζ.

The radial density profiles of the hollow 5 mol % cross-linked microgels, as obtained from the SANS data fitted with the model for hollow fuzzy spheres,[27] are plotted in Figure 4A. As reported elsewhere[27,28,54] after the core dissolution, the cavity is smaller than the initial silica core that had a radius of 57 ± 1 nm.[65] This is observed in both the swollen and collapsed state (blue and red lines in Figure 4A and Figure S6, respectively). The hollow structure is conserved both below and above the VPTT in the dilute state. At 20.0 ± 0.1 °C the outer radius $R = 115 \pm 3$ nm, with an inner (cavity) radius $R_{in} = 26 \pm 1$ nm, while at 40.0 ± 0.1 °C, $R = 57.5 \pm 0.7$ nm and $R_{in} = 21.9 \pm 0.4$ nm.

As soon as the microgels make contact, at $\zeta = 0.64 \pm 0.02$, the polymer is pushed into the cavity, which decreases the microgel size. The outer radius of the microgel is 96 ± 3 nm. A further compression to $\zeta = 0.74 \pm 0.02$ leads to a rearrangement of the polymer within the cavity and a deswelling of the microgel to an outer radius of 87 ± 2 nm.

At the highest concentration we measured, $\zeta = 1.00 \pm 0.03$, the collapse of the fuzzy shell is appreciable, the outer radius drops to 83 ± 2 nm, and the cavity is preserved, as shown by the dashed line in Figure 4A. Interestingly, the cavity undergoes an abrupt collapse at $\zeta = 0.64 \pm 0.02$ relative to the swollen state, but then, for further increase of ζ, the cavity size remains almost constant.

Upon comparison of the radial profiles of the relative polymer volume fraction in Figure 4A with those of the regular 5 mol % cross-linked microgels in Figure 2A, the effect of the cavity on the microgel deswelling is evident: the absence of the cross-linked core leads to a more pronounced compression of the hollow 5 mol % cross-linked microgels with respect to the regular 5 mol % cross-linked microgels. Thus, a hollow microgel deswells more than a regular cross-linked microgel with polymeric networks containing comparable amounts of cross-links. Furthermore, for $\zeta = 1.00 \pm 0.03$, the hollow 5 mol % cross-linked microgels deswell more than regular 2.5 mol % cross-linked and ULC microgels. Introducing a cavity has a greater impact on deswelling at $\zeta \gtrsim 1$ than decreasing the concentration of cross-linker agents used during the synthesis (see Figure S8[65]). In contrast to the case of regular cross-linked microgels embedded within the same matrix, the diameters of the hollow microgels (cyan empty circles) for all the values of ζ probed are smaller than the corresponding d_{nn} (Figure 1), indicating that compression dominates over interpenetration.

To investigate how the interplay between the cavity and the decrease of cross-link concentration within the polymer network affects the deswelling of microgels with increasing ζ, hollow microgels with a 2.5 mol % cross-linked network were embedded in the same matrix as in the previous experiments. Their radial density profiles, as obtained from the fits of the SANS data, are shown in Figure 4B. In the swollen state (blue line), the outer radius of the microgel is 147 ± 4 nm and the cavity has a radius of 24 ± 2 nm. At temperatures above the VPTT, the collapsed microgels have outer radius 55 ± 2 nm and cavity radius 28 ± 2 nm without any external fuzziness, as shown by the red line in Figure S6.

Once the hollow 2.5 mol % cross-linked microgels make contact with the regular microgels in the matrix, their outer radius drops to 102 ± 3 nm already at $\zeta = 0.64 \pm 0.02$, with the cavity shrinking to 10.3 ± 0.9 nm. The overcrowded environment compresses and changes the radial polymer distribution of the hollow 2.5 mol % cross-linked microgels. A further increase of concentration to $\zeta = 0.74 \pm 0.03$ yields a slight decrease of the outer radius to 94 ± 3 nm. The main effect is the collapse of the external fuzzy shell while the internal cavity is preserved and has a size equal to 7.2 ± 0.6

DOI: 10.1021/acs.macromol.9b00729
Macromolecules 2019, 52, 3995−4007

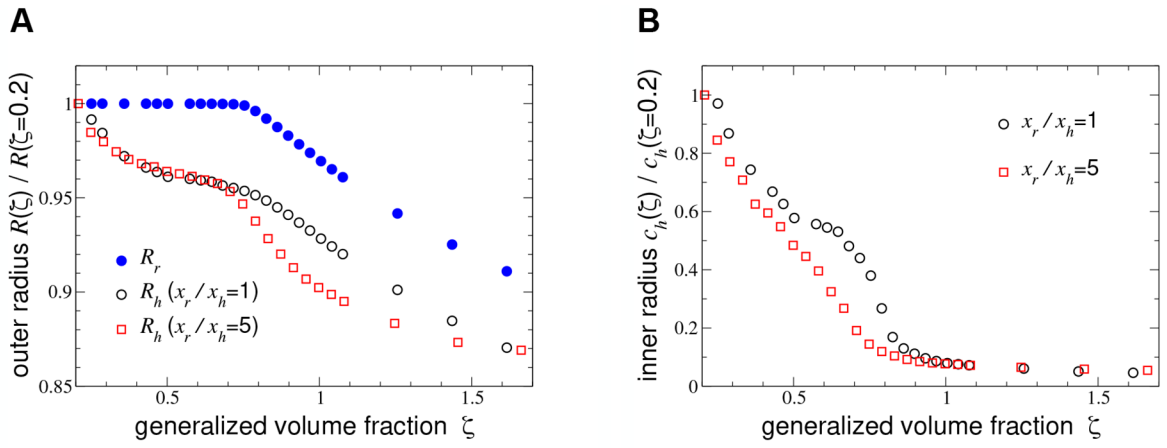

Figure 5. Mean particle radii versus generalized volume fraction in mixtures of regular and hollow microgels with collapsed-state radii R_{0r} = 50 nm, R_{0h} = 50 nm, c_{0h} = 25 nm, Flory solvency parameter χ = 0.2, regular cross-link fraction x_r = 0.001, and two cross-link ratios x_r/x_h. (A) Mean outer radii of regular microgels R_r for x_r = 0.001 (filled circles) and of hollow microgels R_h for x_r/x_h = 1 (empty circles) and 5 (empty squares). (B) Mean inner radii of hollow microgels c_h for x_r/x_h = 1 (empty circles) and 5 (empty squares). Radii are normalized to radius in the reference state, ζ = 0.2. Statistical error bars are smaller than the symbol size.

nm. Finally, at ζ = 1.00 ± 0.04, the cavity is occupied by the internal fuzzy shell. The outer radius measured at this concentration is 87 ± 4 nm.

Comparing the cavity radii of the 2.5 and the 5 mol % hollow microgels reveals that the microgels with fewer cross-links exhibit a more significant collapse of the cavity, which is mainly occupied by the internal fuzzy shell at $\zeta \approx 1.00$ (Figure S9).[65] Similar to the hollow 5 mol % cross-linked microgels, the diameters of the hollow 2.5 mol % microgels (blue empty squares) embedded within the matrix of deuterated microgels are smaller than d_{nn} (Figure 1). Therefore, for all the ζ measured, compression is the dominant response, and no interpenetration is evident.

Monte Carlo Simulations of Mixtures of Microgels. To complement our experimental measurements, we performed Monte Carlo (MC) simulations of a coarse-grained model of microgels, whose swelling is governed by the Flory–Rehner theory of polymer networks[55−57] and whose interparticle interactions are described by Hertz effective pair potentials.[40,65,68] Comparing with experiments requires a large number of microgels to be simulated. Because modeling even a single microgel with explicit polymer chain degrees of freedom can be computationally expensive,[64,69] we represented the microgels simply as elastic spheres whose internal microscopic structure is implicit within the Flory–Rehner single-particle free energy and the Hertz pair potential.[65] For details, see the Flory–Hertz Model of Microgels section. Our aim is to verify whether simulations of this model can reproduce the experimental observation that hollow microgels are more compressed than regularly cross-linked microgels when embedded within a matrix of regular microgels.

Initializing N_h hollow microgels and N_r regular microgels on the sites of a disordered-fcc lattice in a cubic box of fixed volume V with periodic boundary conditions at fixed temperature T, we made trial moves that combined particle displacements and size changes. For visualization, Figure S11[65] shows a typical snapshot. Within the Open Source Physics Library,[70] we implemented the standard Metropolis algorithm,[71,72] accepting a trial displacement and swelling ratio change ($\alpha \rightarrow \alpha'$) with probability $\mathcal{P}_{acc} = \min\{\exp[-(\Delta U + \Delta F)/k_B T]; 1\}$, where ΔU is the change in internal energy associated with interparticle interactions and $\Delta F = F(\alpha') - F(\alpha)$ is the change in polymer network free energy associated with swelling. When moving a hollow microgel, we independently made trial changes in both the inner and outer swelling ratios. As the particles moved and changed size, the Hertz potential amplitudes were updated according to eqs 8−10. After many trial moves, the particles adopt equilibrium configurations and size distributions that minimize the total free energy of the system (see Figure S12[65]).

To explore the dependence of microgel swelling on concentration, we performed a series of simulations, each with N_h = 26 hollow microgels randomly distributed in a matrix of N_r = 230 regular microgels. As input to the simulations, the system parameters that can be varied are the concentrations, collapsed particle radii, cross-link fractions, and Flory χ parameters of the two species. To model aqueous suspensions of pNIPAM, we estimated $\chi \simeq 0.2$ from eq 4, using fit parameters from ref 58. For purposes of illustration, we chose radii R_{0r} = 50 nm, R_{0h} = 50 nm, and c_{0h} = 25 nm for the outer radius of the collapsed regular microgel, the outer radius of the collapsed hollow microgel, and the radius of the cavity of the collapsed hollow microgel, respectively.

Output variables include the swollen radii of the two species as a function of ζ and bulk structural properties of the regular microgel matrix. Over a range of ζ, runs of 10^6 MC steps were performed. After equilibrating for 5×10^4 steps, statistics were collected for particle swelling ratios at intervals of 100 steps.

Figure 5 shows the resulting mean microgel outer radii versus ζ in mixtures of regular microgels of cross-link fraction x_r = 0.001 and hollow microgels of cross-link fractions x_h = 0.001 (x_r/x_h = 1) and x_h = 0.0002 (x_r/x_h = 5). The fully swollen, dilute-limit radii are approximately R_r = 160 nm for regular microgels and R_h = 170 nm, c_h = 90 nm for hollow microgels with x_h = 0.001. These values correspond to swelling ratios roughly comparable to those in the experiments.

As seen in Figure 5A, with increasing concentration, the mean outer radii of both species (R_r and R_h) remain relatively constant up to generalized volume fractions approaching close packing ($\zeta \simeq 0.74$), beyond which they steadily decrease, reflecting concentration-induced deswelling. This trend is in remarkable agreement with the behavior observed experimen-

DOI: 10.1021/acs.macromol.9b00729
Macromolecules 2019, 52, 3995−4007

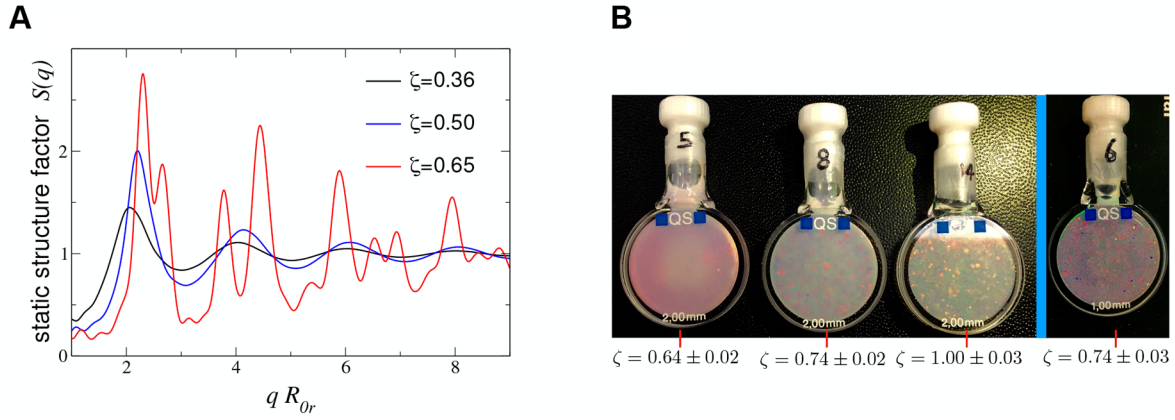

Figure 6. (A) Static structure factor of regular microgels, $S(q)$, versus scattering vector magnitude q for parameters of Figure 5, cross-link ratio x_r/x_h = 1, and generalized volume fractions ζ from fluid (ζ = 0.36) to solid (ζ = 0.65) phases. (B) Images of crystalline samples of the 5 mol % cross-linked microgels in the SANS cuvette, with embedded (from left to right): hollow 5 mol % at ζ = 0.64 ± 0.02, 0.74 ± 0.02, and 1.00 ± 0.03 and hollow 2.5 mol % at ζ = 0.74 ± 0.03.

tally in Figure 1 and Figure S8.[65] Furthermore, the more weakly cross-linked hollow microgels (x_h = 0.0002) deswell more—relative to a reference state of ζ = 0.2—than the more strongly cross-linked hollow microgels (x_h = 0.001). We also performed runs for different values of χ and found qualitatively similar swelling trends.

As seen in Figure 5B, the mean inner (cavity) radius of the hollow particles c_h declines steadily with increasing concentration, beginning already in the dilute state and leveling off around $\zeta \simeq 1$, reflecting rapid collapse of the cavity. As with the outer radii, the inner radii of the softer microgels decrease more—relative to the reference state—than those of their stiffer counterparts. Fluctuations of the inner radii are largest at low concentrations, decreasing with increasing concentration. We conclude that the softer the hollow microgels, the more readily their cavities collapse with increasing concentration of the regular microgel matrix. This trend is in excellent agreement with the experimental results shown in Figure 4 and Figure S9.[65]

Finally, Figure 6A shows the static structure factor of the regular microgel matrix. At lower concentrations, the matrix is in a disordered fluid phase, as reflected by relatively weak oscillations in $S(q)$. In this state, the hollow microgels are only weakly confined and not significantly compressed. The mobility of the regular microgels may account for the larger fluctuations in the cavity radius of the hollow microgels. At higher concentrations, the matrix is in an ordered solid phase, as signaled by distinct peaks in $S(q)$ and the relatively high main peak. In this state the hollow microgels are tightly confined and compressed by their regular microgel neighbors, causing their cavities to collapse.

The crystallization of a majority of regular microgels in the presence of defects with comparable size but different architecture (i.e., the hollow microgels), which we observed in our simulations, is consistent with our observations of crystals, visible to the eye, in the samples measured with SANS. The image in Figure 6B shows four crystalline samples consisting of suspensions with a majority of deuterated regular microgels in which a minority of hollow microgels were dispersed.

CONCLUSIONS

Both experiments and simulations demonstrate that in overcrowded environments of regularly cross-linked microgels the presence of a cavity leads to greater deswelling of the microgels than a decrease in the concentration of cross-linker agents incorporated during synthesis. The cavity offers an alternative way to avoid the energetic cost of neighbors being squeezed together: with increasing compression, the polymer chains can rearrange into the central cavity. This internal freedom allows the hollow microgels to be compressed more than the regular microgels, making compression their dominant response in overcrowded environments of regularly cross-linked microgels.

The cross-link concentration within the polymer network plays a key role in determining the extent to which the cavity is compressed and gradually occupied by the polymer. When hollow microgels have a cross-link concentration comparable to that of the regularly cross-linked microgels in the matrix in which they are embedded (5 mol % or x_r/x_h = 1), the cavity, after first abruptly shrinking, resists further squeezing. In contrast, both the outer and inner radii of hollow microgels, which have lower cross-link fraction (2.5 mol % or x_r/x_h = 5) than their regularly cross-linked neighbors (5 mol %), decrease more rapidly.

Upon comparison of the radial distributions in Figures 2 and 4, it is also evident that for microgels with comparable cross-link concentration the presence of the cavity leads to a more pronounced deswelling at concentrations well above close packing of spheres. Further studies will have to be conducted to probe the behavior of hollow microgels embedded in an environment of hollow microgels. We can speculate that the influence of cross-linking density on deswelling/interpenetration of hollow microgels with different bulk moduli might differ for suspensions of hollow microgels relative to their behavior when embedded in a matrix of regularly cross-linked microgels. In particular, the presence of a cavity instead of a more dense and cross-linked core might lead to more significant interpenetration with respect to deswelling. We argue this since the fuzzy shell is known to be the softest and more penetrable part of a microgel, as shown here by the behavior of the regularly cross-linked microgels and by other studies.[46,48,50] In contrast, the more cross-linked core has a larger polymer density and is less deformable under

DOI: 10.1021/acs.macromol.9b00729
Macromolecules 2019, 52, 3995−4007

compression.[47] Therefore, once microgels are overcrowded, the presence of a dense core limits the possibility for two microgels to further interpenetrate and compression of the fuzzy shell might be favorable. In other words, the presence of a core represents an internal constraint that has been shown to suppress microgel interpenetration.[29] For this reason, we expect hollow microgels to more readily interpenetrate their neighbors when embedded in a matrix of hollow microgels. Whether less cross-linked hollow microgels, when embedded in a matrix of more densely cross-linked hollow microgels, will tend to more easily compress, since they are softer, or interpenetrate, since their fuzzy shell is less cross-linked, is an open question for future study.

Our study highlights that bare knowledge of the amount of cross-linker used during the synthesis is not sufficient to predict the behavior of microgels in overcrowded environments. In other words, the architecture of a microgel must be considered together with the amount of cross-linker to be able to predict whether a microgel is softer than another and whether it interpenetrates or is compressed by its neighbors.

Our findings can be used to rationalize some apparently contrasting results from previous studies. In other related studies,[46,48] microgels with a softness comparable to that of their neighbors were used. For these systems, upon increasing the concentration, only slight deswelling was observed and interpenetration was the dominant response. This case is consistent with our experiments where we mixed the 5 and 2.5 mol % regular microgels and the deuterated 5 mol % regular microgels. Interpenetration of microgels is the dominant response if all the microgels have comparable size and softness.

In contrast, when ultrasoft microgels are embedded within a stiffer matrix, a more pronounced deswelling is observed above a threshold concentration. This trend is consistent with studies in which isotropic deswelling of softer microgels has been observed,[40,45,47,49,68] demonstrating that when the bulk moduli of the microgel species differ significantly, isotropic deswelling dominates over interpenetration. Furthermore, the presence of a cavity determines the prevalence of deswelling over interpenetration both if the polymer network is as stiff as that of the neighboring microgels and if the hollow microgels are softer than the surrounding matrix.

With regards to the possible deformation of the microgels, only the form factors of the hollow microgels showed deviations from the spherical model at very low q (empty triangles versus the solid blue line in Figure 3 for $q < 5 \times 10^{-2}$ nm^{-1} and Supporting Information[65]). These deviations might signal deformation for $\zeta \gtrsim 1$. Therefore, our results seem to support the conclusion of ref 50, regarding microgels with larger size compared to the microgels of our study, that deformation is significant only in highly overcrowded environments. They are also consistent with recent computer simulation data.[64]

Hollow and ultra-low cross-linked microgels represent important model systems for exploring the response of disordered networks to external stimuli.[73,74] Analogies between colloidal gels and biologically important materials, e.g., actin networks in living cells,[75] have already elucidated the behavior of the cytoskeleton in cellular functions.[76] The capability to design microgels that mainly collapse (hollow microgels) or interpenetrate (regular microgels with different cross-linker concentration and distribution) will allow to obtain suspensions with the desired viscosity and yield stress.[77] This capability is pivotal for using those suspensions as substrates for 3D printing.[10−12] Our experiments and simulations advance such efforts by clearly demonstrating that deswelling of microgels in overcrowded environments can be enhanced more by introducing a solvent-filled cavity than by reducing the concentration of cross-linker agents during the particle synthesis. Finally, our finding that mixing microgels of similar size but different architecture does not hinder crystallization demonstrates the potential to realize crystals with a new kind of defect that will respond uniquely to both crowding and changes of external stimuli. Furthermore, the effect of topology and interpenetration/deswelling on crystallization can be studied using mixtures of hollow microgels with different cross-linker densities and sizes. As mentioned above, we expect that interpenetration between neighbors will be the dominant effect for hollow microgels embedded in a matrix of hollow microgels. Whether this mechanism will hinder crystallization is unclear and should be studied in the future. Furthermore, it is reasonable to assume that differences in size and bulk moduli between hollow microgels in suspensions play a key role, allowing for variation of the size distribution due to the compression of the larger/softer hollow microgels, as observed for regular microgels.[47,78] Such size variation can either occur at concentrations where microgels are mobile or well above jamming concentrations. In the first case, the size change facilitates crystallization[49], while in the latter microgels are jammed and cannot rearrange, as for ultra-low cross-linked microgels confined at a fluid interface.[20]

■ ASSOCIATED CONTENT

Supporting Information

The Supporting Information is available free of charge on the ACS Publications website at DOI: 10.1021/acs.macromol.9b00729.

Form factor model; SAXS data and analysis; viscosimetry data and analysis; SANS data and analysis; Monte Carlo simulation details; Table S1: sample name, label of the synthesized batch, values of the conversion constants and of the radii, and polydispersities as determined by SANS; Figure 1: SAXS form factor and data fit of the sacrificial silica core; Figure S2: SAXS scattered intensity, form factor, and structure factors with fits of the first peak; Figure S3: viscosimetry data and fits; Figure S4: experimental determination of match point of neutron scattering length density of the deuterated microgels; Figure S5: SANS form factors and fits; Figure S6: radial distributions as determined from the SANS data fit; Figure S7: comparison between fits with different models; Figure S8: radii of the different microgels determined by SANS as a function of ζ; Figure S9: radii of the internal cavity for the different hollow microgels determined by SANS as a function of ζ; Figure S10: swelling ratio for all the samples; Figure S11: snapshot from a simulation; Figure S12: probability distributions of microgel swelling ratios (PDF)

■ AUTHOR INFORMATION

Corresponding Authors

*E-mail: andrea.scotti@rwth-aachen.de.

*E-mail: richtering@rwth-aachen.de.

ORCID

Andrea Scotti: 0000-0002-8988-330X

Monia Brugnoni: 0000-0003-2220-3645

DOI: 10.1021/acs.macromol.9b00729
Macromolecules 2019, 52, 3995−4007

Judith E. Houston: 0000-0001-5205-3620
Ralf Schweins: 0000-0001-8078-2089
Igor I. Potemkin: 0000-0002-6687-7732
Walter Richtering: 0000-0003-4592-8171

Author Contributions

A.S. and W.R. designed the research. A.R.D. performed MC simulations. A.S. performed the experiments and analyzed the data. M.B. synthesized the microgels. M.B., J.E.H., and R.S. helped with SANS measurements. All authors contributed to the manuscript.

Notes

The authors declare no competing financial interest.
All the data used for this paper are available, under request, at https://hdl.handle.net/21.11102/1807a70e-208f-11e9-9660-e41f1366df48. SANS data collected at ILL are available at doi: 10.5291/ILL-DATA.9-11-1855.

■ ACKNOWLEDGMENTS

The authors are thankful to Dr. A. Menzel and to the EUSMI program for the help with the measurements performed on the cSAXS beamline. A.S. thanks F. M. Schulte, M. M. Schmidt, and S. Bochenek for the help during SAXS and SANS experiments. Financial support from the Alexander von Humboldt Foundation, the Deutsche Forschungsgemeinschaft within SFB 985 - Functional Microgels and Microgel Systems, the International Helmholtz Research School of Biophysics and Soft Matter (IHRS BioSoft), and the Government of Russian Federation within Act 211, Contract 02.A03.21.0011, is gratefully acknowledged. This work is based upon experiments performed at the KWS-2 instrument operated by JCNS at the Heinz Maier-Leibnitz Zentrum (MLZ), Garching, Germany, and at the D11 instrument at the Institut Laue-Langevin (ILL), Grenoble, France (doi: 10.5291/ILL-DATA.9-11-1855). SAXS data were taken on the cSAXS beamline of the Swiss Light Source, Paul Scherrer Institut. ILL (Fill2030 campaign) agreed to sponsor the open access or this article.

■ REFERENCES

(1) Plamper, F. A.; Richtering, W. Functional Microgels and Microgel Systems. *Acc. Chem. Res.* **2017**, *50*, 131−140.
(2) Karg, M.; Pich, A.; Hellweg, T.; Hoare, T.; Lyon, L. A.; Crassous, J. J.; Suzuki, D.; Gumerov, R. A.; Schneider, S.; Potemkin, I. I.; Richtering, W. Nanogels and Microgels: From Model Colloids to Applications, Recent Developments, and Future Trends. *Langmuir* **2019**, *35*, 6231.
(3) Omidinia-Anarkoli, A.; Boesveld, S.; Tuvshindorj, U.; Rose, J. C.; Haraszti, T.; De Laporte, L. An Injectable Hybrid Hydrogel with Oriented Short Fibers Induces Unidirectional Growth of Functional Nerve Cells. *Small* **2017**, *13*, 1702207.
(4) Rose, J. C.; Cámara-Torres, M.; Rahimi, K.; Köhler, J.; Möller, M.; De Laporte, L. Nerve Cells Decide to Orient inside an Injectable Hydrogel with Minimal Structural Guidance. *Nano Lett.* **2017**, *17*, 3782−3791.
(5) Guerzoni, L. P. B.; Bohl, J.; Jans, A.; Rose, J. C.; Koehler, J.; Kuehne, A. J. C.; De Laporte, L. Microfluidic fabrication of polyethylene glycol microgel capsules with tailored properties for the delivery of biomolecules. *Biomater. Sci.* **2017**, *5*, 1549−1557.
(6) Ben, Y.; Robb, I.; Tonmukayakul, P.; Wang, Q. In *Microgel Suspensions: Fundamentals and Applications*; Fernandez-Nieves, A., Wyss, H., Mattsson, J., Weitz, D., Eds.; Wiley-VCH Verlag GmbH & Co. KGaA: 2011.
(7) Uhlig, K.; Wegener, T.; He, J.; Zeiser, M.; Bookhold, J.; Dewald, I.; Godino, N.; Jaeger, M.; Hellweg, T.; Fery, A.; Duschl, C. Patterned Thermoresponsive Microgel Coatings for Noninvasive Processing of Adherent Cells. *Biomacromolecules* **2016**, *17*, 1110−1116.
(8) Menut, P.; Seiffert, S.; Sprakel, J.; Weitz, D. A. Does size matter? Elasticity of compressed suspensions of colloidal- and granular-scale microgels. *Soft Matter* **2012**, *8*, 156−164.
(9) Kunz, S.; Pawlik, M.; Schärtl, W.; Seiffert, S. Polymer- vs. colloidal-type viscoelastic mechanics of microgel pastes. *Colloid Polym. Sci.* **2018**, *296*, 1341−1352.
(10) Bhattacharjee, T.; Zehnder, S. M.; Rowe, K. G.; Jain, S.; Nixon, R. M.; Sawyer, W. G.; Angelini, T. E. Writing in the granular gel medium. *Science advances* **2015**, *1*, e1500655.
(11) Bhattacharjee, T.; Gil, C. J.; Marshall, S. L.; Uruena, J. M.; O'Bryan, C. S.; Carstens, M.; Keselowsky, B.; Palmer, G. D.; Ghivizzani, S.; Gibbs, C. P.; Sawyer, W. G.; Angelini, T. E. Liquid-like Solids Support Cells in 3D. *ACS Biomater. Sci. Eng.* **2016**, *2*, 1787−1795.
(12) O'Bryan, C. S.; Bhattacharjee, T.; Niemi, S. R.; Balachandar, S.; Baldwin, N.; Ellison, S. T.; Taylor, C. R.; Sawyer, W. G.; Angelini, T. E. Three-dimensional printing with sacrificial materials for soft matter manufacturing. *MRS Bull.* **2017**, *42*, 571−577.
(13) Lyon, L. A.; Fernandez-Nieves, A. The Polymer/Colloid Duality of Microgel Suspensions. *Annu. Rev. Phys. Chem.* **2012**, *63*, 25−43.
(14) Stieger, M.; Pedersen, J. S.; Lindner, P.; Richtering, W. Are Thermoresponsive Microgels Model Systems for Concentrated Colloidal Suspensions? A Rheology and Small-Angle Neutron Scattering Study. *Langmuir* **2004**, *20*, 7283−7292.
(15) Fernandez-Nieves, A.; Fernandez-Barbero, A.; Vincent, B.; de las Nieves, F. J. Charge Controlled Swelling of Microgel Particles. *Macromolecules* **2000**, *33*, 2114−2118.
(16) Cors, M.; Wrede, O.; Genix, A.-C.; Anselmetti, D.; Oberdisse, J.; Hellweg, T. Core-Shell Microgel-Based Surface Coatings with Linear Thermoresponse. *Langmuir* **2017**, *33*, 6804−6811.
(17) Cors, M.; Wiehemeier, L.; Hertle, Y.; Feoktystov, A.; Cousin, F.; Hellweg, T.; Oberdisse, J. Determination of Internal Density Profiles of Smart Acrylamide-Based Microgels by Small-Angle Neutron Scattering: A Multishell Reverse Monte Carlo Approach. *Langmuir* **2018**, *34*, 15403−15415.
(18) Gumerov, R. A.; Rumyantsev, A. M.; Rudov, A. A.; Pich, A.; Richtering, W.; Möller, M.; Potemkin, I. I. Mixing of Two Immiscible Liquids within the Polymer Microgel Adsorbed at Their Interface. *ACS Macro Lett.* **2016**, *5*, 612−616.
(19) Camerin, F.; Fernández-Rodríguez, M. A.; Rovigatti, L.; Antonopoulou, M.-N.; Gnan, N.; Ninarello, A.; Isa, L.; Zaccarelli, E. Microgels Adsorbed at Liquid-Liquid Interfaces: A Joint Numerical and Experimental Study. *ACS Nano* **2019**, *13*, 4548−4559.
(20) Scotti, A.; Bochenek, S.; Brugnoni, M.; Fernandez-Rodriguez, M. A.; Schulte, M. F.; Houston, J. E.; Gelissen, A. P. H.; Potemkin, I. I.; Isa, L.; Richtering, W. Exploring the colloid-to-polymer transition for ultra-low crosslinked microgels from three to two dimensions. *Nat. Commun.* **2019**, *10*, 1418.
(21) Brown, A. C.; Stabenfeldt, S. E.; Ahn, R. T.; Dhada, K. S.; Herman, E. S.; Stefanelli, V.; Guzzetta, N.; Alexeev, A.; Lam, W. A.; Lyon, L. A.; Barker, T. H. Ultrasoft microgels displaying emergent platelet-like behaviours. *Nat. Mater.* **2014**, *13*, 1108.
(22) Sigolaeva, L. V.; Gladyr, S. Y.; Mergel, O.; Gelissen, A. P. H.; Noyong, M.; Simon, U.; Pergushov, D. V.; Kurochkin, I. N.; Plamper, F. A.; Richtering, W. Easy-Preparable Butyrylcholinesterase/Microgel Construct for Facilitated Organophosphate Biosensing. *Anal. Chem.* **2017**, *89*, 6091−6098.
(23) Matsui, S.; Kureha, T.; Hiroshige, S.; Shibata, M.; Uchihashi, T.; Suzuki, D. Fast Adsorption of Soft Hydrogel Microspheres on Solid Surfaces in Aqueous Solution. *Angew. Chem., Int. Ed.* **2017**, *56*, 12146−12149.
(24) Douglas, A. M.; Fragkopoulos, A. A.; Gaines, M. K.; Lyon, L. A.; Fernandez-Nieves, A.; Barker, T. H. Dynamic assembly of ultrasoft colloidal networks enables cell invasion within restrictive fibrillar polymers. *Proc. Natl. Acad. Sci. U. S. A.* **2017**, *114*, 885−890.

DOI: 10.1021/acs.macromol.9b00729
Macromolecules 2019, 52, 3995−4007

(25) Zha, L.; Zhang, Y.; Yang, W.; Fu, S. Monodisperse Temperature-Sensitive Microcontainers. *Adv. Mater.* **2002**, *14*, 1090−1092.
(26) Nayak, S.; Gan, D.; Serpe, M. J.; Lyon, L. A. Hollow Thermoresponsive Microgels. *Small* **2005**, *1*, 416−421.
(27) Dubbert, J.; Honold, T.; Pedersen, J. S.; Radulescu, A.; Drechsler, M.; Karg, M.; Richtering, W. How hollow are thermoresponsive hollow nanogels? *Macromolecules* **2014**, *47*, 8700−8708.
(28) Schmid, A. J.; Dubbert, J.; Rudov, A. A.; Pedersen, J. S.; Lindner, P.; Karg, M.; Potemkin, I. I.; Richtering, W. Multi-Shell Hollow Nanogels with Responsive Shell Permeability. *Sci. Rep.* **2016**, *6*, 22736.
(29) Brugnoni, M.; Scotti, A.; Rudov, A. A.; Gelissen, A. P. H.; Caumanns, T.; Radulescu, A.; Eckert, T.; Pich, A.; Potemkin, I. I.; Richtering, W. Swelling of a Responsive Network within Different Constraints in Multi-Thermosensitive Microgels. *Macromolecules* **2018**, *51*, 2662−2671.
(30) Moncho-Jordá, A.; Germán-Bellod, A.; Angioletti-Uberti, S.; Adroher-Benítez, I.; Dzubiella, J. Nonequilibrium Uptake Kinetics of Molecular Cargo into Hollow Hydrogels Tuned by Electrosteric Interactions. *ACS Nano* **2019**, *13*, 1603−1616.
(31) Trappe, V.; Prasad, V.; Cipelletti, L.; Segre, P. N.; Weitz, D. A. Jamming phase diagram for attractive particles. *Nature* **2001**, *411*, 772.
(32) Zhang, Z.; Xu, N.; Chen, D. T. N.; Yunker, P.; Alsayed, A. M.; Aptowicz, K. B.; Habdas, P.; Liu, A. J.; Nagel, S. R.; Yodh, A. G. Thermal vestige of the zero-temperature jamming transition. *Nature* **2009**, *459*, 230.
(33) Paloli, D.; Mohanty, P. S.; Crassous, J. J.; Zaccarelli, E.; Schurtenberger, P. Fluid-solid transitions in soft-repulsive colloids. *Soft Matter* **2013**, *9*, 3000−3004.
(34) van der Scheer, P.; van de Laar, T.; van der Gucht, J.; Vlassopoulos, D.; Sprakel, J. Fragility and Strength in Nanoparticle Glasses. *ACS Nano* **2017**, *11*, 6755−6763.
(35) Mattsson, J.; Wyss, H. M.; Fernandez-Nieves, A.; Miyazaki, K.; Hu, Z.; Reichman, D. R.; Weitz, D. A. Soft colloids make strong glasses. *Nature* **2009**, *462*, 83−86.
(36) Keidel, R.; Ghavami, A.; Lugo, D. M.; Lotze, G.; Virtanen, O.; Beumers, P.; Pedersen, J. S.; Bardow, A.; Winkler, R. G.; Richtering, W. Time-resolved structural evolution during the collapse of responsive hydrogels: The microgel-to-particle transition. *Science Advances* **2018**, *4*, eaao7086.
(37) Ma, X.; Davidson, Z. S.; Still, T.; Ivancic, R. J. S.; Schoenholz, S. S.; Liu, A. J.; Yodh, A. G. Heterogeneous Activation, Local Structure, and Softness in Supercooled Colloidal Liquids. *Phys. Rev. Lett.* **2019**, *122*, 028001.
(38) Senff, H.; Richtering, W. Temperature sensitive microgel suspensions: Colloidal phase behavior and rheology of soft spheres. *J. Chem. Phys.* **1999**, *111*, 1705−1711.
(39) Debord, S.; Lyon, L. A. Influence of Particle Volume Fraction on Packing in Responsive Hydrogel Colloidal Crystals. *J. Phys. Chem. B* **2003**, *107*, 2927−2932.
(40) Urich, M.; Denton, A. R. Swelling, structure, and phase stability of compressible microgels. *Soft Matter* **2016**, *12*, 9086−9094.
(41) Stieger, M.; Richtering, W.; Pedersen, J.; Lindner, P. Small-angle neutron scattering study of structural changes in temperature sensitive microgel colloids. *J. Chem. Phys.* **2004**, *120*, 6197−6206.
(42) Senff, H.; Richtering, W. Influence of cross-linker density on rheological properties of temperature-sensitive microgel suspensions. *Colloid Polym. Sci.* **2000**, *278*, 830−840.
(43) Mohanty, P.; Richtering, W. Structural Ordering and Phase Behavior of Charged Microgels. *J. Phys. Chem. B* **2008**, *112*, 14692−14697.
(44) Gasser, U.; Lietor-Santos, J.-J.; Scotti, A.; Bunk, O.; Menzel, A.; Fernandez-Nieves, A. Transient formation of bcc crystals in suspensions of poly(N-isopropylacrylamide)-based microgels. *Phys. Rev. E* **2013**, *88*, 052308.
(45) Iyer, A. S. J.; Lyon, L. A. Self-Healing Colloidal Crystals. *Angew. Chem., Int. Ed.* **2009**, *48*, 4562−4566.
(46) Gasser, U.; Hyatt, J. S.; Lietor-Santos, J.-J.; Herman, E. S.; Lyon, L. A.; Fernandez-Nieves, A. Form factor of pNIPAM microgels in overpacked states. *J. Chem. Phys.* **2014**, *141*, 034901.
(47) Scotti, A.; Gasser, U.; Herman, E. S.; Pelaez-Fernandez, M.; Lyon, L. A.; Fernandez-Nieves, A.; et al. The role of ions in the self-healing behavior of soft particle suspensions. *Proc. Natl. Acad. Sci. U. S. A.* **2016**, *113*, 5576−5581.
(48) Mohanty, P. S.; Nöjd, S.; van Gruijthuijsen, K.; Crassous, J. J.; Obiols-Rabasa, M.; Schweins, R.; Stradner, A.; Schurtenberger, P. Interpenetration of polymeric microgels at ultrahigh densities. *Sci. Rep.* **2017**, *7*, 1487.
(49) Scotti, A.; Gasser, U.; Herman, E. S.; Han, J.; Menzel, A.; Lyon, L. A.; Fernandez-Nieves, A. Phase behavior of binary and polydisperse suspensions of compressible microgels controlled by selective particle deswelling. *Phys. Rev. E: Stat. Phys., Plasmas, Fluids, Relat. Interdiscip. Top.* **2017**, *96*, 032609.
(50) Conley, G. M.; Aebischer, P.; Nöjd, S.; Schurtenberger, P.; Scheffold, F. Jamming and overpacking fuzzy microgels: Deformation, interpenetration, and compression. *Science Advances* **2017**, *3*, e1700969.
(51) Bouhid de Aguiar, I.; van de Laar, T.; Meireles, M.; Bouchoux, A.; Sprakel, J.; Schroën, K. Deswelling and deformation of microgels in concentrated packings. *Sci. Rep.* **2017**, *7*, 10223.
(52) Virtanen, O. L. J.; Mourran, A.; Pinard, P. T.; Richtering, W. Persulfate initiated ultra-low cross-linked poly(N-isopropylacrylamide) microgels possess an unusual inverted cross-linking structure. *Soft Matter* **2016**, *12*, 3919−3928.
(53) Stöber, W.; Fink, A.; Bohn, E. Controlled growth of monodisperse silica spheres in the micron size range. *J. Colloid Interface Sci.* **1968**, *26*, 62−69.
(54) Dubbert, J.; Nothdurft, K.; Karg, M.; Richtering, W. Core-shell-shell and hollow double-shell microgels with advanced temperature responsiveness. *Macromol. Rapid Commun.* **2015**, *36*, 159−164.
(55) Flory, P. J. *Principles of Polymer Chemistry*; Cornell University Press: Ithaca, NY, 1953.
(56) Flory, P. J.; Rehner, J. Statistical Mechanics of Cross-Linked Polymer Networks I. Rubberlike Elasticity. *J. Chem. Phys.* **1943**, *11*, 512−520.
(57) Flory, P. J.; Rehner, J. Statistical Mechanics of Cross-Linked Polymer Networks II. Swelling. *J. Chem. Phys.* **1943**, *11*, 521−526.
(58) Fernandez-Barbero, A.; Fernandez-Nieves, A.; Grillo, I.; Lopez-Cabarcos, E. Structural modifications in the swelling of inhomogeneous microgels by light and neutron scattering. *Phys. Rev. E: Stat. Phys., Plasmas, Fluids, Relat. Interdiscip. Top.* **2002**, *66*, 051803.
(59) Lopez, C. G.; Richtering, W. Does Flory-Rehner theory quantitatively describe the swelling of thermoresponsive microgels? *Soft Matter* **2017**, *13*, 8271−8280.
(60) Landau, L. D.; Lifshitz, E. M. *Theory of Elasticity*, 3rd ed.; Elsevier: Amsterdam, 1986.
(61) de Gennes, P.-G. *Scaling Concepts in Polymer Physics*; Cornell University Press: Ithaca, NY, 1979.
(62) Gao, J.; Frisken, B. J. Cross-Linker-Free N-Isopropylacrylamide Gel Nanospheres. *Langmuir* **2003**, *19*, 5212−5216.
(63) Brugnoni, M.; Nickel, A. C.; Kroger, L. C.; Scotti, A.; Pich, A.; Leonhard, K.; Richtering, W. Synthesis and structure of deuterated ultra-low cross-linked poly(N-isopropylacrylamide) microgels. *Polym. Chem.* **2019**, *10*, 2397−2405.
(64) Scotti, A.; Brugnoni, M.; Rudov, A. A.; Houston, J. E.; Potemkin, I. I.; Richtering, W. Hollow microgels squeezed in overcrowded environments. *J. Chem. Phys.* **2018**, *148*, 174903.
(65) See the Supporting Information.
(66) Romeo, G.; Imperiali, L.; Kim, J.-W.; Fernandez-Nieves, A.; Weitz, D. A. Origin of de-swelling and dynamics of dense ionic microgel suspensions. *J. Chem. Phys.* **2012**, *136*, 124905.
(67) Berndt, I.; Pedersen, J. S.; Richtering, W. Structure of Multiresponsive "Intelligent" Core-Shell Microgels. *J. Am. Chem. Soc.* **2005**, *127*, 9372−9373.

DOI: 10.1021/acs.macromol.9b00729
Macromolecules 2019, 52, 3995−4007

(68) Weyer, T. J.; Denton, A. R. Concentration-dependent swelling and structure of ionic microgels: Simulation and theory of a coarse-grained model. *Soft Matter* **2018**, *14*, 4530−4540.
(69) Gnan, N.; Rovigatti, L.; Bergman, M.; Zaccarelli, E. In Silico Synthesis of Microgel Particles. *Macromolecules* **2017**, *50*, 8777−8786.
(70) Gould, H.; Tobochnik, J.; Christian, W. *Introduction to Computer Simulation Methods*; Addison-Wesley: Boston, MA, 2006.
(71) Frenkel, D.; Smit, B. *Understanding Molecular Simulation*, 2nd ed.; Academic: London, 2001.
(72) Binder, K.; Heermann, D. W. *Monte Carlo Simulation in Statistical Physics: An Introduction*, 5th ed.; Springer: Berlin, 2010.
(73) Vermeulen, M. F. J.; Bose, A.; Storm, C.; Ellenbroek, W. G. Geometry and the onset of rigidity in a disordered network. *Phys. Rev. E: Stat. Phys., Plasmas, Fluids, Relat. Interdiscip. Top.* **2017**, *96*, 053003.
(74) Wilhelm, J.; Frey, E. Elasticity of Stiff Polymer Networks. *Phys. Rev. Lett.* **2003**, *91*, 108103.
(75) Gardel, M. L.; Shin, J. H.; MacKintosh, F. C.; Mahadevan, L.; Matsudaira, P. A.; Weitz, D. A. Scaling of F-Actin Network Rheology to Probe Single Filament Elasticity and Dynamics. *Phys. Rev. Lett.* **2004**, *93*, 188102.
(76) Gardel, M. L.; Shin, J. H.; MacKintosh, F. C.; Mahadevan, L.; Matsudaira, P.; Weitz, D. A. Elastic Behavior of Cross-Linked and Bundled Actin Networks. *Science* **2004**, *304*, 1301−1305.
(77) Conley, G. M.; Harden, J. L.; Scheffold, F. Relationship between Rheology and Structure of Interpenetrating, Deforming and Compressing Microgels. arXiv e-prints 2018, arXiv:1811.01657.
(78) Gasser, U.; Scotti, A.; Fernandez-Nieves, A. Spontaneous deswelling of microgels controlled by counterion clouds. *Phys. Rev. E: Stat. Phys., Plasmas, Fluids, Relat. Interdiscip. Top.* **2019**, *99*, 042602.

DOI: 10.1021/acs.macromol.9b00729
Macromolecules 2019, 52, 3995−4007